A study of very high resolution visible spectra of Titan: Line characterisation in visible CH4 bands and the search for C3

Rafael Rianço-Silva, Pedro Machado, Zita Martins, Emmanuel Lellouch, Jean-Christophe Loison, Michel Dobrijevic, João A. Dias, José Ribeiro

Planetary and Space Science 240 (2024) 105836

Contents lists available at ScienceDirect

Planetary and Space Science

journal homepage: www.elsevier.com/locate/pss

A study of very high resolution visible spectra of Titan: Line characterisation in visible CH_4 bands and the search for C_3

Rafael Rianço-Silva [a,b], Pedro Machado [a,b,*], Zita Martins [c], Emmanuel Lellouch [d], Jean-Christophe Loison [e], Michel Dobrijevic [f], João A. Dias [a,b], José Ribeiro [a,b]

[a] Institute of Astrophysics and Space Sciences, Observatório Astronómico de Lisboa, Ed. Leste, Tapada da Ajuda, 1349-018 Lisbon, Portugal
[b] Faculty of Sciences, University of Lisbon, Portugal
[c] Centro de Química Estrutural, Institute of Molecular Sciences and Department of Chemical Engineering, Instituto Superior Técnico, Universidade de Lisboa, Portugal
[d] LESIA, Observatoire de Paris, PSL Research University, CNRS, Sorbonne Universités, Université de Paris, France
[e] Institut des Sciences Moléculaires (ISM), CNRS, Univ. Bordeaux, France
[f] Laboratoire d'Astrophysique de Bordeaux, Univ. Bordeaux, CNRS, France

ARTICLE INFO

Keywords:
Titan
High resolution visible spectroscopy
Minor chemical species
Methane
Chemical retrieval of planetary atmospheres
Photochemistry
C_3

ABSTRACT

The atmosphere of Titan is a unique natural laboratory for the study of atmospheric evolution and photochemistry akin to that of the primitive Earth, with a wide array of complex molecules discovered through infrared and sub-mm spectroscopy. Here, we explore high resolution visible spectra of Titan (obtained with VLT-UVES) and retrieve an empirical high resolution list of methane absorption features at high resolution, (R = 100.000) between 5250 Å and 6180 Å, for which no linelists are yet available. Furthermore, we search for the predicted, but previously undetected carbon trimer, C_3, on the atmosphere of Titan, at its 4051 Å band. Our results are consistent with the presence of C_3 at the upper atmosphere of Titan, with a column density of 10^{13} cm^{-2}. This study of Titan's atmosphere with high-resolution visible spectroscopy presents a unique opportunity to observe a planetary atmosphere where CH_4 is the main visible molecular absorber, from which CH_4 optical proprieties can be studied. It also showcases the use of a close planetary target to test new methods for chemical retrieval of minor atmospheric compounds, in preparation for upcoming studies of cold terrestrial exoplanet atmospheres.

1. Introduction

Home to a thick and chemically diverse atmosphere, Titan stands out among the giant planet's icy satellites, as one of the most thoroughly studied objects in the solar system (Sánchez-Lavega, 2011; Hörst, 2017). Distinct observations and space missions have constrained Titan's atmospheric contents to be of a bulk (> 94% by mass) N_2, alongside a significant amount of CH_4 (5% by mass at the troposphere) (Sánchez-Lavega, 2011; Hörst, 2017). Alongside this bulk N_2–CH_4 atmosphere, observing Titan's atmosphere has revealed a diverse array of photochemically generated hydrocarbon and nitrile species that condense into optically thick global haze layers, as a result of photochemical dissociation of CH_4 (and to a smaller extent, N_2) on Titan's upper atmosphere (Sánchez-Lavega, 2011; Hörst, 2017; Coustenis et al., 2007; Nixon et al., 2013). Complementary theoretical studies have also been conducted to model chemical species, chemical pathways and vertical profiles, in order to replicate observations and obtain new predictions that can be further tested with new data (Hérbad et al., 2013; Dobrijevic et al., 2016; Vuitton et al., 2019).

After the end of the Cassini mission, ground-based observations have been used to further constrain Titan's trace atmospheric compounds, detecting new chemical species. This has been mostly done with sub-mm arrays such as the Atacama Large Millimetre Array (ALMA), retrieving the presence of species such as ethyl cyanide (C_2H_5CN in 2015) (Cordiner et al., 2015), vinyl cyanide (C_2H_3CN in 2017) (Palmer et al., 2017), and cyclopropenylidene (c-C_3H_2, in 2020) (Nixon et al., 2020) - or with the use of high-resolution infrared spectroscopy, as was the case of the discovery of propadiene (CH_2CCH_2, in 2019), from observations with NASA infrared Telescope Facility-Texas Echelon Cross Echelle Spectrograph (IRTF-TEXES) (Lombardo et al., 2019).

Intense molecular spectral features populating infrared bands can be identified using high resolution infrared spectroscopy, making it

* Corresponding author at: Faculty of Sciences, University of Lisbon, Portugal.
E-mail addresses: rdsilva@fc.ul.pt (R. Rianço-Silva), pmmachado@fc.ul.pt (P. Machado).

https://doi.org/10.1016/j.pss.2023.105836
Received 28 July 2023; Received in revised form 4 November 2023; Accepted 28 December 2023
Available online 8 January 2024

an excellent tool to discover new molecules on chemically complex planetary atmospheres (Lombardo et al., 2019; Hanel et al., 2003; Encrenaz et al., 2010). Nonetheless, molecular transitions are not limited to infrared wavelengths, with some molecules providing examples of rich visible spectra. However, due to the higher energies involved, associated with reduced absorption cross-sections, obtaining detailed, high resolution linelists for molecules in shorter visible wavelengths is challenging (Hargreaves et al., 2020; Gordon et al., 2022). An example of this lack of detailed knowledge regarding the high resolution nature of visible molecular bands is that of methane's visible spectrum, for which no high resolution, line-by-line linelist exists for wavelengths below 7460 Å (Hargreaves et al., 2020) even though several methane absorption bands are known at shorter wavelengths, such as the 6190 Å, 5970 Å, 5760 Å and 5430 Å bands (Giver, 1978; Smith et al., 1990; Karkoschka, 1994; Karkoschka and Tomasko, 2010).

Atmospheric methane is regarded as a molecule of geochemical and astrobiological interest in terrestrial planets and icy worlds (Thompson et al., 2022). This is since, for habitable zone rocky planets around Sun-like stars, atmospheric methane photochemical lifetime is expected to be short (< 1 Myr) in geological timescales, and hence its presence in the atmosphere requires an active replenishment source (Thompson et al., 2022). Its astrobiological potential is, in part, rooted in the fact that most of Earth's atmospheric methane is biogenic in origin, at least since Archean Earth (Thompson et al., 2022), but also due to this gas thermodynamic instability when combined with oxidising species such as CO_2 in a rocky planet's atmosphere (Thompson et al., 2022; Krissansen-Totton et al., 2018). This suggests that large quantities of atmospheric CO_2 and CH_4 in a terrestrial planet's atmosphere are unlikely to coexist without a biological source of CH_4, particularly when observed in the absence of CO (Thompson et al., 2022; Krissansen-Totton et al., 2018).

Indeed, the detection of CH_4 in Mars' atmosphere at ppb levels (with significant temporal and spatial variability) has sparked the debate of whether the origin of gas was geochemical (through underground serpentinisation reactions) or biological (by subsurface methanogenic martian microorganisms) (Krasnopolsky et al., 2004; Formisano et al., 2004). At the same time, the irreversible photolysis of CH_4 on Titan's atmosphere (sparking its complex atmospheric photochemistry) also points towards a geochemical replenishment mechanism such as outgassing from interior CH_4 clathrate hydrates (Tobie et al., 2009). With such a relevant role for the study of planetary geochemical cycles in icy moons and as a possible biosignature in rocky planets atmospheres, the search for CH_4 spectral features in exoplanet atmospheres became a key driver for the development of new infrared observatories such as the James Webb Space Telescope (JWST) (Gialluca et al., 2021) or the future Atmospheric Remote-sensing infrared Exoplanet Large-survey (ARIEL) mission (Tinetti et al., 2018).

Ground-based visible high resolution spectroscopy of exoplanet atmospheres (with a resolving power high enough to allow to discern individual absorption lines) may provide complementary information from the one obtained by moderate resolution (R ≈ 1000) infrared observatories such as JWST and ARIEL, once detailed linelist for visible bands of CH_4 are available (Hargreaves et al., 2020). High resolution visible spectra of an atmosphere such as Titan's may allow the characterisation of the line by line nature of these bands, as methane is the sole major visible molecular absorber in Titan's atmosphere (Sánchez-Lavega, 2011; McKay et al., 2001). As a solar system target with a methane-rich atmosphere, Titan offers a testing ground for future high resolution spectroscopy observations of small and cold exoplanet atmospheres.

Another molecule with an interesting visible absorption spectrum is the tricarbon molecule C_3, marked by the most intense $\tilde{A}^1\Pi_u$ - $\tilde{X}^1\Sigma_g^+$ 000–000 band at 4051 Å. It was originally detected on a cometary coma (Gausset et al., 1965), subsequently found in circumstellar shells (Hinkle et al., 1988) and, more recently, detected in diffuse interstellar clouds by the high-resolution ground-based Very Large Telescope-UV–Visual Echelle Spectrograph (VLT-UVES) (Dekker et al., 2000), observing individual C_3 absorption lines part of the 4051 Å band in interstellar cloud (Roueff et al., 2002; Schmidt et al., 2014). This species is also produced in carbon-cluster experiments (Hinkle et al., 1988; Schmidt et al., 2014). It has, nonetheless, never previously been detected on a planetary atmosphere (Hérbad et al., 2013).

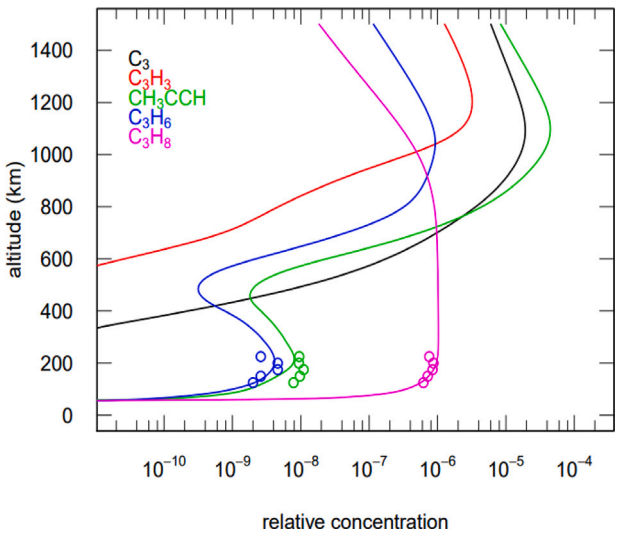

Fig. 1. Molar fraction vertical profiles of the main C_3H_p species on Titan's Atmosphere — including carbon trimer C_3, as one of the most abundant C_3H_p carbon species above altitudes of 600 km, following Hérbad et al. (2013) model (Hérbad et al., 2013). Comparison with Nixon et al. (2013) abundance retrievals of CH_3CCH, C_3H_6 and C_3H_8 Titan's stratosphere (Nixon et al., 2013).

Interest in this triatomic carbon carbon species on Titan's atmosphere emerged as Hérbad et al. (2013) introduced this species in a more complete model of C_3H_p hydrocarbon photochemistry for Titan's atmosphere, in order to constrain heavier hydrocarbon chemistry on this environment. On their model, C_3 is mostly produced on Titan's upper atmosphere by the reaction of abundant acetylene (C_2H_2) with atomic carbon (Hérbad et al., 2013) as

$$C + C_2H_2 \longrightarrow C_3 + H_2 \quad (1)$$

The results obtained from these photochemical models predict that due to its relative stability, carbon trimer C_3 should be one of the most abundant C_3H_p species in Titan's mesosphere and thermosphere alongside propyne (CH_3CCH), reaching molar fractions above 10 ppm at altitudes of 800 km, (Hérbad et al., 2013; Dobrijevic et al., 2016) as it is shown in Fig. 1. A previous search for the C_3 4051 Å band in solar occultation mode archived Cassini/VIMS data had been conducted by D'Aversa et al. (2017). However, the low resolution of the VIMS instrument (~7 nm at 400 nm) could not allow the study of individual absorption lines, in order to detect a trace chemical species such as C_3.

Hence, in this article we present the analysis of dedicated high spectral resolution ($R = 100.000$) observations of Titan visible methane bands with VLT-UVES and a new method for spectral line characterisation. These allowed to retrieve a list of new CH_4 absorption lines at the previously uncharacterised visible CH_4 bands here presented. This is complemented by the observations of Titan with VLT-UVES ($R = 60.000$) in search for the previously undetected tricarbon molecule, C_3, through the detection of its strongest absorption band, at 4051 Å. To confirm the presence (or infer the absence above a lower limit) of the photochemical product C_3 in the upper atmosphere of Titan would provide a rather significant observational constraint to the photochemical models used to explain the chemical pathways occurring on Titan's atmosphere. A better understanding of Titan's photochemistry provides a clearer picture of the processes that lead to the formation of the

complex organic molecules which cluster into the organic haze particles that cover Titan's globe (Hörst, 2017), a process that is known to share similarities with some of the proposed mechanisms for endogenous atmospheric abiotic synthesis of organic molecules on early Earth (Hörst et al., 2012).

2. Observations and data reduction

Dedicated observations of Titan with the blue Arm of the UVES instrument at the 8.2 m Unit 2 Telescope of the Very Large Telescope (VLT) (Dekker et al., 2000) were obtained on the night of 21/06/2018. The observations were conducted with a seeing limit of 0".80 and an instrument slit width of 0".7, implying a spectral resolving power of R = 60,000 (Dekker et al., 2000). These observations were complemented in this study with archived observations with the red arm of the same instrument from Luz et al. (2006) in four nights of January 2005, conducted with a seeing limit of 0.80". Since Titan's apparent diameter was of 0".78 in the 2018 campaign and of 0.88" in the 2005 campaign, we are limited in these observations to disk-averaged spectra. Still, due to the lower instrument width of 0".3, these observations were conducted with a spectral resolving power of $R = 100,000$ (Dekker et al., 2000).

Table 1 summarises some characteristics of the spectral observations of Titan used in this study, divided in 2005 UVES red arm spectra (4200 Å to 6186 Å), Luz et al. (2006) and 2018 UVES blue arm spectra (3800 Å to 4800 Å), both with a wavelength bin of 0.015 Å. These observations were processed from its raw form using ESOReflex pipeline for VLT-UVES spectra. Each exposure is processed individually, following bias and dark removal as well as flat-fielding, as described in Luz et al. (2006). This process also allowed the wavelength calibration - based on the instrument's Th-Ar lamp exposures - and flux calibration of the spectral data - obtained with the EsoReflex pipeline using the detector's master response curve to convert the measured detector signal to physical flux units. This further led to the obtention of a matrix containing each pixel's flux errors (in flux units), based on the photonic noise as well as the instrumental noise, retrieved from the flat, bias and dark exposures used by this data reduction pipeline.

The distinct spectral orders obtained in each UVES echellogram exposure were combined into single 2-D spectra of Titan, each with both flux and flux error values associated, for each exposure. One of the matrix's axis (corresponding to the dispersion direction, alongside the slit's width) is associated with the wavelength axis. In the other direction, alongside the slit's length, each pixel corresponds to a distinct spacial position in the sky, with the edges showing background sky and the centre showcasing the disk of Titan.

With a pixel scale of 0.25" in the 2018 Titan observations, the disk of Titan covered three pixels in the spacial direction of the 2D spectrum. Hence, a disk-integrated spectrum was obtained for the 2018 observations by averaging the three spectra covering the disk of Titan. Similarly, with a pixel scale of 0.18", disk-integrated spectra of 2005 observations implied averaging the five central spectra of the 2D spectrum that covered the entirety of disk of Titan. For each observation night, all disk-integrated exposures were also averaged into one single 1D disk-integrated spectrum of Titan per observation night. Since each observation night corresponds to a distinct average radial velocity between the Earth and Titan (3rd column of Table 1), a distinct Doppler shift correction was applied to each night's averaged 1D spectrum, correcting these spectra to the rest frame of Titan.

Unlike the 2005 red arm observations, all of the 2018 blue arm exposures were taken during the same night. This causes its processing and usage to be far more straightforward, since all the previously mentioned calibration steps can be conducted simultaneously for consecutive exposures within the same observation - while exposures taken in distinct observation nights - as those obtained in the 2005 campaign - require independent calibration (from different calibration exposures that were taken at each observing night). Thus, we are left with five disk and night averaged visible spectra of Titan, Doppler shifted to Titan's rest frame: One spectrum combining all 2018 VLT-UVES blue arm observations and four 2005 VLT-UVES red arm spectra, one per each observation night.

Due to the distinct radial velocities between the Sun and Titan on the distinct observation nights (4th column of Table 1), distinct Doppler shifts are observed in the solar absorption lines present on Titan's visible spectra (5th column of Table 1). This prevents us from combining nightly spectra into a single spectrum with increased signal to noise ratio (SNR), since solar absorption features appear significantly shifted with respect to each other (Figs. 4 and 5). However, as we describe ahead, this Doppler shift in solar lines presents an advantage in line characterisation of visible spectra of planetary atmospheres.

In order to allow a comparison and interpretation of these high-resolution visible spectra of Titan (resulting from backscattered solar light) the solar spectrum in high resolution from the BASS2000 solar spectrum survey is used — obtained in the ground-based International Scientific Station of the Jungfraujoch (Aboudarham and Renié, 2020) with a resolution of 0.002 Å. These spectrum's telluric absorption lines were not removed and provide a useful basis for comparison with this study's ground-based observations that did not endure telluric line removal as well.

3. The Doppler method for spectral line identification

The wavelength range covered by the 2005 VLT-UVES red arm observations of Titan (4200 Å-6186 Å) is known to cover a set of weak methane absorption bands, such as the 6190 Å, 5970 Å, 5760 Å and 5430 Å CH_4 bands (Giver, 1978). Although these absorption bands have been known for decades (Giver, 1978), and their presence identified in all of the solar system gas giant atmospheres (Karkoschka, 1994), these bands are not yet characterised in high resolution, and hence, no knowledge of these band's line-by-line structure is available (Bourdon et al., 2009; Karkoschka and Tomasko, 2010). Our understanding of the high-resolution structure of visible CH_4 bands is, therefore, severely incomplete compared with infrared CH_4 bands, for which spectroscopic databases exist above 746 nm (Hargreaves et al., 2020), listing the known molecular transitions that cause absorption lines present in high resolution spectra of CH4-bearing atmospheres.

It has not yet been possible to empirically characterise the line-by-line visible CH_4 spectrum due to the weak absorption bands in laboratory, given their very reduced absorption cross-section (of 4×10^{-26} cm^{-2} at 540 nm compared with the stronger NIR CH_4 absorption bands at 1.2×10^{-23} cm^{-2} at 890 nm (Giver, 1978; He et al., 2021)), requiring hundreds of kilometers of atmosphere pathlengths to imprint their presence on a spectrum (Karkoschka and Tomasko, 2010; Bourdon et al., 2009). Theoretical characterisation of CH_4 molecular transitions in visible wavelengths has also proven challenging given the exceedingly complex nature of CH_4 high frequency excited vibrational energy levels (polyads) (Bourdon et al., 2009). To tackle this issue, high resolution (R = 100.000) observations of Titan – the only Solar System atmosphere where CH_4 is the sole main molecular visible absorber (Sánchez-Lavega, 2011; McKay et al., 2001) – are used in this work to allow the detection and characterisation of individual CH_4 lines that compose these high frequency uncharacterised bands.

CH_4 is the sole molecular species whose absorption bands have previously been identified in Titan's visible spectrum (Karkoschka and Tomasko, 2010; McKay et al., 2001). However, when observing at high resolution (R = 100,000), we expect to find the CH_4 absorption lines composing its absorption bands overlaid on top of the backscattered solar spectrum. At these resolutions, it implies that solar absorption lines (including the deep Fraunhofer lines) are expected to be found in the same spectral sections as the previously uncharacterised CH_4 lines we aim to detect (Machado et al., 2014). It is thus imperative to distinguish between Titan's atmosphere absorption features and solar absorption lines. This can be done by comparing Titan's spectrum with an equally

Table 1
VLT-UVES Observations of Titan used in the context of this work. The first rows corresponds to the ones obtained in 2005 by Luz et al. (2006) using UVES red arm (4200 Å to 6186 Å), while the last row accounts for the dedicated observations of Titan with UVES blue arm (3800 Å to 4800 Å). Velocity values retrieved from NASA/JPL HORIZONS ephemeris calculator. Redshift of solar lines with relation to the solar rest frame on each spectrum, at Titan's rest frame were considered at 5000 Å for red arm observations and at 4000 Å for blue arm observations.

Date	Exposures	Titan-Earth velocity (m/s)	Titan-Sun velocity (m/s)	Solar redshift (mÅ)
08/01/2005	8 (red arm)	+4710 ± 30	−1500 ± 50	−25 ± 1
13/01/2005	9 (red arm)	−4180 ± 120	−3740 ± 20	−62 ± 1
15/01/2005	8 (red arm)	−610 ± 130	−160 ± 50	−3 ± 1
16/01/2005	9 (red arm)	+3240 ± 160	+1920 ± 60	+32 ± 1
21/06/2018	22 (blue arm)	+1040 ± 240	+4140 ± 70	+56 ± 1

high resolution solar spectrum, resolving individual solar absorption lines, such as the BASS2000 solar spectral database (with a spectral resolution of 0.002 Å) (Aboudarham and Renié, 2020). It is worth mentioning that similarly to the spectral observations of Titan, the solar spectrum used for calibration is also obtained from a ground-based observatory, and from whose spectrum telluric absorption lines were not removed — allowing a comparison with the observed spectrum solar and telluric lines.

Nonetheless, it is possible to take advantage of the four distinct nights of observation of Titan, and use their relative solar Doppler shift to distinguish between solar and Titan absorption lines. Indeed, visual comparison between the distinct observation nightly spectra (Figs. 4 and 5) evidences the distinct aspect of Doppler shifted solar lines versus Titan-originated unshifted lines. As expected, the same solar absorption line (sharing their spectral position with the lines present at the solar database, black line in Figs. 4 and 5) appears shifted on distinct observation nights. In fact, these nightly solar line Doppler shifts correspond to the expected shifts from Titan-Sun velocities at the observing nights. Solar lines observed at 13/01/2005 are the most blueshifted (by 4 to 5 wavelength bins, corresponding to the −62 mÅ Doppler shift with respect to the rest frame), while 16/01/2005 lines are the most redshifted (by 1 to 3 wavelength bins, corresponding to +32 mÅ with respect to the rest frame) at wavelength bins of 15 mÅ. At the same time, other lines – which do not appear to correspond to any solar feature present at the solar database – are all superimposed at the same position. This suggests that these lines are not subject to the sun's distinct radial velocities with respect to Titan, being originated instead from Titan's rest frame. We propose to use this fact to detect absorption lines originated in Titan's atmosphere in a visible spectrum amid backscattered solar lines. To do so, it is necessary to possess several spectra of the atmosphere of interest observed at times when the planet's radial velocity with respect to the sun is different.

To search for this shift among distinct nightly spectra, we firstly removed the continuum component of the observational spectra (by applying a median filter to each spectral point, assigning it the median value of it and its 300 nearest neighbours) and normalised sections of interest of Titan's spectra by dividing the night and disk-integrated spectra by this continuum, preparing for our Doppler Line Identification method to be applied. The normalised spectrum provides Titan's atmosphere transmittance spectrum (due molecular absorption) down to an optically thick reflecting layer, $T(\lambda)$.

Applying this new method, we firstly obtained a list of all absorption lines in each normalised spectra (by finding the inversion points, of derivative 0, in each spectra). Then, all points on all four spectral line lists were compared, with our code selecting only spectral lines whose line centres on the four observation nights are not separated to their equivalent lines on other observation nights by a distance greater than the minimum Doppler shift between 2 observation nights. In this case, this minimum shift between 2 absorption lines corresponds to the shift of 22 mÅ (between observation nights 8/1/2005 and 15/1/2005) plus the Doppler shift's uncertainty as 25 mÅ. Any absorption lines found to differ by more than 25 mÅ between any two observation nights are discarded as solar absorption line. Finally, each of the "detected" line's position was calculated from the mean of the four respective line positions in the four observation nights, as well as its depth with respect to its immediate neighbourhood continuum and its full width at half maximum (FWHM). In addition, we have considered only detected lines with a relative depth of at least 2% of the continuum, as a way to avoid spurious line detections (by the algorithm finding derivative 0 points at the spectrum) as we shall discuss in Section 6.1.

This list of all spectral lines whose central position has not shifted by more than 25 mÅ over the course of different nights of observation, shall correspond to absorption features originating from the rest frame of Titan. A list of corresponding line depth (with respect to the continuum) for selected lines has also been obtained from the mean of line depth from the distinct nights of observation. Measuring the average FWHM for each of Titan's spectral lines, and assuming a Gaussian line profile, for optically thin lines, it is possible to estimate each detected Titan line's Equivalent Width (EW) through Eq. (2).

$$\mathrm{EW} = \text{Line Depth} \cdot \frac{\sqrt{\pi}}{2\sqrt{\ln(2)}} \cdot \mathrm{FWHM} \tag{2}$$

In order to estimate the intrinsic line strength of each detected line, S_{ij}, in cm^{-1}. (molecule. $\mathrm{cm}^{-2})^{-1}$ units, we have compared the observed spectra to a set of synthetic spectra of Titan, whereupon these newly detected lines are simulated for different intrinsic line strengths. To obtain these synthetic spectra, we approximate Titan's haze to a single backscattering layer model of this atmosphere occurring at Titan's optical radius (the distance from the centre of the planet at which the planetary atmosphere becomes optically thin, that we fixed in our model at 200 km of altitude for λ = 600 nm following Lorenz et al. (1999)). In this simple model, we approximate the effect of atmospheric molecular absorption as if it were caused by a single uniform atmospheric layer containing the molecular absorber above Titan's optical radius, while assuming that the entirety of haze backscattering occurs at Titan's optical radius (Lorenz et al., 1999). We have also assumed that that CH_4 lines are approximated by a Gaussian profile, whose cross-section as a function of wavelength is given by Eq. (3).

$$\sigma_{ij}(\lambda) = \frac{S_{ij}}{\gamma_D\sqrt{\pi}} \exp\left[-\left(\frac{\lambda-\lambda_0}{\gamma_D}\right)^2\right] \tag{3}$$

As a first approximation, all spectral lines are simulated with the same Full Width at Half Maximum (FWHM) due to Doppler Broadening (Eq. (4)).

$$\mathrm{FWHM} = 2\gamma_D\sqrt{\ln 2} = \frac{2\lambda_0}{c}\sqrt{\frac{2k_B T \ln 2}{m_{\mathrm{CH_4}}}} \tag{4}$$

Multiplying the line profile cross-section by the one-way column density of CH_4 (N) down to Titan's optical radius provides the optical depth as a function of wavelength of an individual spectral line. We consider a 2-way, disk-averaged airmass of 3, accounting for the 2-way path of light down to the optically thick layer where backscattering is assumed to occur, as an average for the entirety of the disk. Considering this, the synthetic transmittance spectrum of the newly detected lines within these CH_4 bands are obtained by multiplying each line's individual transmittance curve, by Eq. (5).

$$T(\lambda) = \prod_{j\to i} e^{-3\tau_{ij}(\lambda)} = \prod_{j\to i} e^{-3N\sigma_{ij}(\lambda)}\ , \text{ since } \tau_{ij}(\lambda) = N\sigma_{ij}(\lambda) \tag{5}$$

This set of synthetic transmittance spectra of CH_4 lines are convoluted by a Gaussian profile to match the detector's resolution, and then multiplied by an average spectrum of the VLT-UVES red arm observations where the new CH_4 spectral lines identified by this Doppler Method have been removed. This allows to compare the line bottom of these newly detected lines in VLT-UVES spectra of Titan to the line bottom in several synthetic spectra of varying intrinsic line strength — providing an estimate of the detected CH_4 lines' strength based on the best match between VLT-UVES lines' and synthetic lines' bottom, as can be observed in Figure S1 of Supplementary Information. The final list of the detected Titan CH_4 absorption lines and respective line depth, EW and Intrinsic Strength estimation will be analysed in the results Section 5.1. It is worth noticing that a small fraction of the detected CH_4 absorption lines may coincide with shallower solar absorption lines. This implies that although line detection still holds valid, the estimation of spectral line strength as described above will be affected by the coincidence with the solar absorption lines — leading to deeper absorption lines than what should be solely caused by molecular absorption in Titan. Hence, it was decided to include a further criterion to exclude from line strength estimation Titan absorption lines that may be affected by solar absorption: Titan spectral lines whose centre is separated from a solar spectral line (deeper than 2% of continuum) by less than the detector's resolution (0,06 Å) were excluded from line strength estimation.

4. Methods for detection of minor atmospheric compounds

The search for the 4051 Å absorption band of C_3 in Titan was conducted on the 2018 VLT-UVES blue Arm observations as these cover the spectral region of interest. Since all exposures were obtained in the same night, the novel method described in is not applicable in the 2018 data.

Dias et al. (2022) describe a simple and straightforward method of detection of minor chemical species using the radiative transfer suite Planetary Spectrum Generator (Villanueva et al., 2018). By simulating atmospheric spectra with variable abundances of the molecule of interest, it is possible to compare spectral features caused by this molecule in the conditions of the observed planetary atmosphere with observational spectra — allowing the detection of this chemical species on that planetary atmosphere, as well as estimating its abundance (Dias et al., 2022). In Negative detection cases, this method allows to estimate upper-limits for the studied species' abundance in the observed atmospheric layers. However, given the lack of high-resolution k-tables that model the transmission spectra of C_3, it is not possible to automatically simulate Titan spectra with C_3, neither with PSG nor with other radiative transfer suites such as NEMESIS (Irwin et al., 2008).

The transmittance spectrum of C_3 under the conditions of Titan shall therefore be obtained in an approximated way, based on the C_3 band oscillator strength and expected column density. Previous photochemical modelling work on Titan's atmosphere have predicted C_3 column density on Titan's upper atmosphere to be $N = 5.6 \times 10^{13}$ cm^{-2}, with a minimum expected column density extending down to $N = 5.0 \times 10^{12}$ cm^{-2} (Hérbad et al., 2013 and Dobrijevic et al., 2016).

Resorting to this prediction and the C_3 4051 Å band line list empirically obtained by Schmidt et al. (2014) (table S1, on supplementary information), the first approximation synthetic C_3 transmittance spectra for Titan were obtained (Fig. 2). To do so, individual C_3 oscillator strengths, f_J, on table S1, were firstly multiplied by the population distribution in rotational energy levels, J, as a function of temperature, which in a first approximation is provided through Eq. (6), where for C_3, $B = 0.431$ cm^{-1}, from Tanabashi et al. (2005).

$$\mathrm{pop}(J) = (2J+1)\exp\left[-\frac{hcBJ(J+1)}{k_B T}\right] \tag{6}$$

From this product, it is possible to obtain each individual line's strength (S_{ij}) at their central wavelength value (λ_0) within the (000)-(000) C_3 visible band from Eq. (7), equivalent to the spectral integral of each individual transition's cross-section, $\sigma(\lambda)$. Using each line's intrinsic strength value, S_{ij}, a profile for each line's cross-section, $\sigma(\lambda)$, is obtained assuming a Doppler broadened, or Gaussian profile (Eq. (3)).

$$S_{ij} = \int_0^\infty \sigma(\lambda) d\lambda = \frac{e^2 \lambda_0^2}{4 m_e c^2 \varepsilon_0} \mathrm{pop}(J).f_J \tag{7}$$

Finally, it is possible to obtain the optical depth profile ($\tau_{ij}(\lambda)$) as well as the spectral Transmission profile ($T_{ij}(\lambda)$) for each spectral line through Eq. (5). These individual spectral line profiles are then multiplied, allowing a spectral model of the C_3 band to be simulated as a function of one-way C_3 column density (N) as is shown in Fig. 2, for a disk-integrated, 2-way, airmass = 3, atmosphere of Titan, similarly to what is done for the analysis of line strength of newly detected CH_4 lines, described above.

Again, all spectral lines are simulated with the same FWHM due to Doppler Broadening (Eq. (4)), which, for $\lambda_0 \sim 4050$ Å and $T \sim 150$ K at altitudes of 1000 km in Titan (where C_3 abundances are predicted to be higher (Hérbad et al., 2013; Dobrijevic et al., 2016)) accounting for Doppler broadened C_3 line FWHM of ~ 0.006 Å. However, given the resolving power of $R = 60{,}000$ of the spectrograph used in these observations, we expect a spectral resolution no better than $\lambda/R = 0.06$ Å. Therefore we convoluted the synthetic spectra with a Gaussian filter, in order to obtain a synthetic spectrum with the same spectral resolution as the VLT-UVES spectra of Titan. Examples of two synthetic transmittance spectra for C_3 adjusted to the observations spectral resolution are compared in Fig. 2 - one for the Dobrijevic et al. (2016) model standard one-way column density value ($N = 5.6 \times 10^{13}$ cm^{-2}) and another for its minimum predicted value ($N = 5.0 \times 10^{12}$ cm^{-2}).

As mentioned above, it is critical to have a solar spectrum of equivalent resolution to compare the observations with. However, and unlike the search for individual CH_4 visible lines, for the search for C_3 spectral features, the VLT-UVES Titan spectrum was not normalised by its continuum since we are interested in probing only a small wavelength range of interest corresponding to the C_3 4051 Å absorption band. For the solar spectrum to be directly comparable with the observed Titan spectrum, the solar spectrum was instead normalised by its local maximum. This is a valid approximation to Titan's spectrum without any molecular absorber (an OFF spectrum (Dias et al., 2022)) since Titan's backscattered spectrum is dominated by haze scattering and absorption which, in this short wavelength range (4050 Å to 4055 Å), evolves slowly with wavelength (McKay et al., 2001) as spectral features due to aerosols are broad with no fine line structure, unlike gases. More concretely, from 5000 Å to 4000 Å, the effect of haze absorption reduces Titan's albedo by 40% along a wavelength range of 1000 Å, McKay et al. (2001) or, as a continuous absorption, causes a decrease in radiance of 0,04% per Å. Hence, haze continuous absorption and scattering effects are negligible at the tens of Angstrom-sized wavelength ranges covered by the normalised spectral sections we compare here. To allow this comparison, the solar spectrum was also convoluted to our instrumental resolution and Doppler shifted by the Titan-Sun relative velocity at the observation time — so that solar lines match, as it is evident in Fig. 6.

By multiplying this solar proxy for Titan's spectrum by the transmission spectrum of C_3, we produce a first approximation synthetic Titan spectrum with C_3 (an ON spectrum), enabling the comparison of these two ON-OFF models for Titan spectra (with and without C_3 absorption features) with the observational spectrum of Titan — allowing search for non-solar spectral features coinciding with C_3 absorption lines as described in the Results Section 5.2.

5. Results

5.1. Line-by-line detection on visible methane bands

The previously described Doppler Method for Spectral line identification was applied to four spectral regions that are known to contain

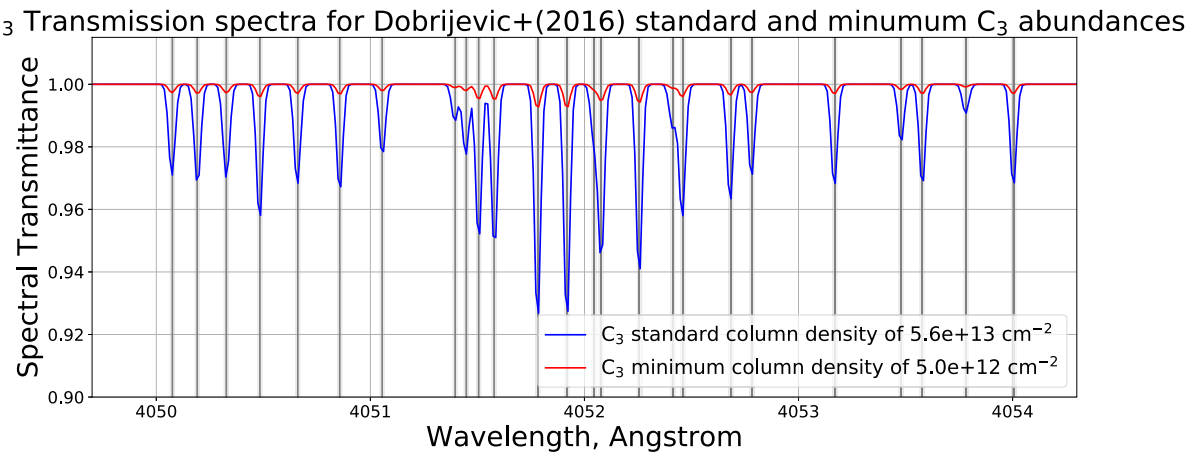

Fig. 2. C_3 synthetic spectra of its 4051 Å $\tilde{A}^1\Pi_u$ - $\tilde{X}^1\Sigma_g^+$ 000-000 vibronic band. The blue spectrum corresponds to a C_3 column density in Titan's upper atmosphere of 5.6×10^{13} cm^{-2} equal to the median value predicted by Dobrijevic et al. (2016) photochemical model. Red spectrum corresponds to the minimum value for C_3 column abundance expected by the same photochemical model, 5.0×10^{12} cm^{-2}. Vertical grey lines correspond to C_3 line centres and respective uncertainty of ±0.01 Å identified in Schmidt et al. (2014).

CH_4 absorption bands whose individual line-by-line structure was yet to be characterised in high resolution. Previous spectral studies aimed at characterising these visible CH_4 bands did not reach resolving powers above $R = 2000$, and hence were incapable of resolving individual CH_4 lines (Karkoschka and Tomasko, 2010). These bands are shown in Fig. 3 as regions where the observed spectral continuum is reduced, due to overlap of many weak CH_4 absorption lines. Our two key detection threshold parameters were: Maximum line centre distance of 25 mÅ between all distinct observation nights (all line positions in different observation nights shall fall within a span of 25 mÅ) and a minimum relative line depth value of 2% (which amounts to 10 times the value of the typical flux errorbar per wavelength bin, of 0.2% of the continuum at 3σ, and 5 times of the typical line depth uncertainty of 0.4%). An analysis of the impact of the line depth threshold is presented in the Discussion and Conclusions Section 6.1. These are strict criteria that are expected to exclude some potential non-solar lines — with our main concern being to avoid false positive non-solar line detections.

On Figs. 4 and 5 we compare sections of the four normalised nightly spectra with 3σ errorbars (containing the most intense detected Titan absorption features) with a normalised solar spectrum — and mark with black triangles the lines detected by our method. Fig. 4 shows line detections at the 5430 Å CH_4 band whereas Fig. 5 showcases line detections at the relatively stronger 6190 Å CH_4 band. A total of 87 non-solar lines were found on the region covered by the 6190 Å CH_4 band, while only eight non-solar lines were detected at the region covered by the 5430 Å CH_4 band.

On Tables 2 and 3 we showcase examples of non-solar line detections, as the top five deeper absorption lines detected by our Doppler Line identification method at two regions of interest, near 5430 Å and 6190 Å bands. Following the criterion of removing from line strength estimation detected lines that coincided with solar spectral lines within the detector's resolution (0,06 Å), 6 of the 87 detected lines at the 6190 Å band were excluded from line strength estimation. These tables also showcase the calculated EW for each line (in cm^{-1} units), as well as the estimation for intrinsic line strength, in cm/molecule units.

To estimate the intrinsic line strength of the detected lines at the CH_4 absorption bands, we have fitted synthetic spectra of varying line strength (S_{ij}) considering a fixed CH_4 one-way column density of 4.9×10^{21} molecules.cm^{-2}. This CH_4 column density was obtained by integrating Teanby et al. (2006) vertical profile of CH_4 in Titan from the top of the atmosphere down to Titan's optical radius (at an altitude of 200 km over the solid globe of Titan where we assume all incoming sunlight backscattering occurs). This integration of CH_4 number density $n(z)$ in altitude to obtain the one-way column density of CH_4 down to altitude z follows Lellouch et al. (2022), correction for atmospheric sphericity dependent on Titan's radius (R_{Titan}) in Eq. (8).

$$N(z) = \int_z^{\infty} n(z') \left(1 + \frac{z'}{R_{Titan}}\right)^2 dz' \tag{8}$$

Measurements of the optical radius of Titan showcase significant temporal variability ranging from altitudes above Titan's surface of 150 km to 300 km at 600 nm, from 1989 to 1997 (Lorenz et al., 1999) with half of the measurements clustering within 10 km of an optical radius value of 200 km, which is the value we have considered for this study. Hence, we have considered a temporally and spatially invariant atmospheric profile of CH_4 in our integration of the column density of CH_4 in Titan, as a first approximation approach that discards the effect of CH_4 variability on Titan's atmosphere.

Although this detection method was also applied to the even weaker 5760 Å and 5970 Å CH_4 absorption bands (with CH4 absorption coefficients below 10^{-26} cm^{-2} (He et al., 2021)), the smaller line depth of absorption lines (below our detection threshold of relative line depth of 2%) has prevented the detection on these bands of lines in amounts similar to those detected at the deeper 5430 Å and 6190 Å bands. With these criteria, our algorithm only detected one absorption line at each of these two CH_4 bands. The complete list of all detected lines at the four regions of interest are displayed as supplementary materials: the complete detected absorption feature list for the interest region of 5430 Å band is found in table S2, for 5760 Å interest region in table S3, for 5970 Å interest region in table S4, and for 6190 Å interest region in table S5. Applying our method to the entirety of the VLT-UVES red arm Titan spectrum (from 4200 Å - 6186 Å), no extra non-solar absorption line was detected using our method beyond the predicted range of CH_4 bands.

5.2. Search for C_3 absorption features

We shall now compare VLT-UVES Titan spectrum with the solar spectrum (a proxy for Titan's backscattered OFF spectrum, with no molecular absorption) and with the synthetic Titan spectrum which combines this backscattered solar radiation with synthetic C_3 absorption lines (ON spectrum). In this first case, we considered a C_3 column density in Titan's upper atmosphere equal to the predicted 5.6×10^{13} cm^{-2} by Hérbad et al. (2013) and Dobrijevic et al. (2016) photochemical model, shown in Fig. 6.

From this comparison, it is clear that the deep expected spectral absorption features for this C_3 abundance in Titan's atmosphere (in red, reaching depths of 10% of the continuum) are not present in the VLT-UVES disk-integrated spectrum of Titan (black). No comparable

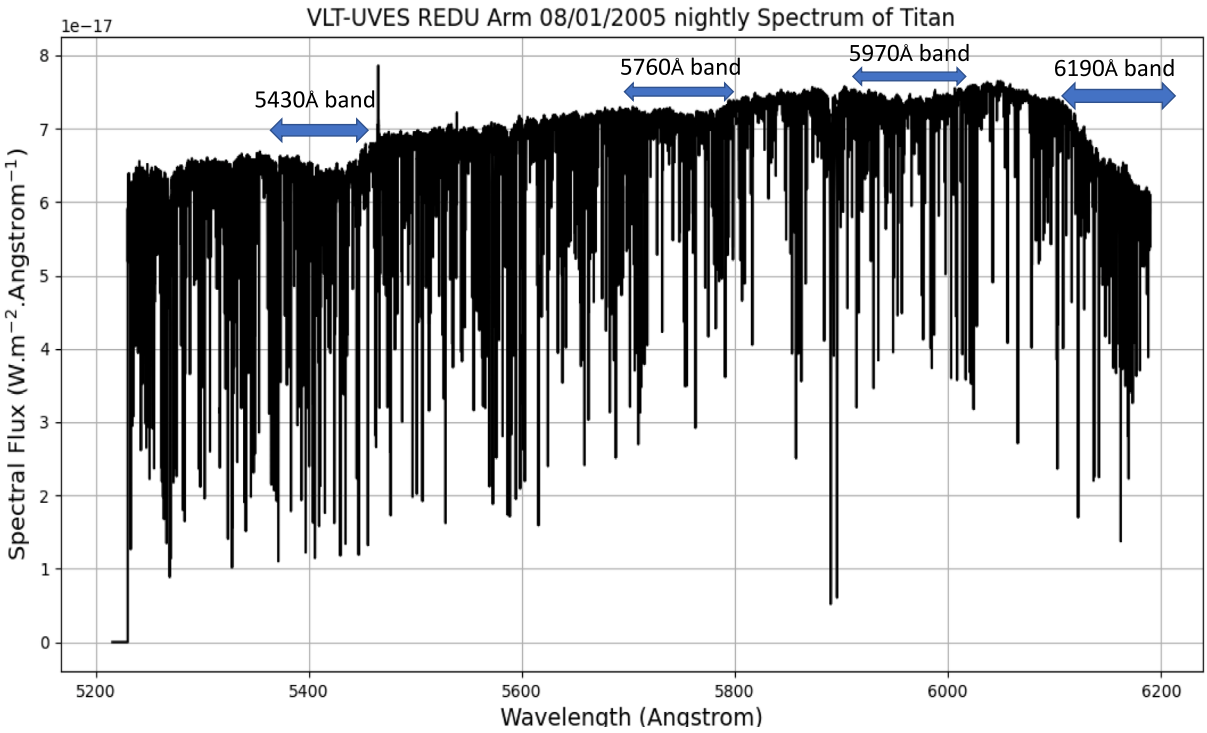

Fig. 3. VLT-UVES REDU disk-integrated, night-averaged spectrum of Titan from Luz et al. (2006), from the 08/01/2005 observation night. This spectrum covers the wavelength range from 5250 Å to 6186 Å, with four CH_4 absorption visible bands (5430 Å, 5760 Å, 5970 Å, 6190 Å). The 6190 Å is the most intense visible absorption CH_4 band in this wavelength range as described in Giver (1978) and Karkoschka and Tomasko (2010).

Table 2
List of five deeper detected lines by our method at the spectral section comprising the weak CH_4 5430 Å absorption band. Many of these lines are shown detected at the spectral plot of Fig. 4. These spectral lines are likely part of the $6\nu_1+\nu_3$ CH_4 band as described by Giver et al. (1978) (Giver, 1978). The supplementary information table S2 is a complete table with all eight detected non-solar lines at the weak CH_4 5430 Å absorption band.

Line	Wavelength (Å)	Relative line depth (%)	Line EW (cm^{-1})	Line strength, S_{ij}, (cm/molec)
1	5427.013 ± 0.017	3.84 ± 0.30	0.0112 ± 0.0030	(2.5 ± 1.0) × 10^{25}
2	5449.492 ± 0.020	2.40 ± 0.36	0.0066 ± 0.0023	(1.0 ± 0.5) × 10^{25}
3	5430.753 ± 0.019	2.39 ± 0.32	0.0093 ± 0.0039	(1.5 ± 0.5) × 10^{25}
4	5433.989 ± 0.013	2.25 ± 0.61	0.0053 ± 0.0027	(1.5 ± 0.5) × 10^{25}
5	5427.487 ± 0.023	2.10 ± 0.14	0.0058 ± 0.0015	(1.5 ± 0.5) × 10^{25}

Table 3
Most of these lines are shown detected at the spectral plot of Fig. 5. These spectral lines are likely part of the $5\nu_1+\nu_3$ CH_4 band as described by Giver et al. (1978) (Giver, 1978). The supplementary information table S5 is a complete table with all 87 detected non-solar lines at the weak CH_4 6190 Å absorption band.

Line	Wavelength (Å)	Relative line depth (%)	Line EW (cm^{-1})	Line strength, S_{ij}, (cm/molec)
1	6182.207 ± 0.010	13.81 ± 0.26	0.0326 ± 0.0065	(8.5 ± 0.5) × 10^{-25}
2	6183.907 ± 0.009	10.58 ± 0.44	0.0204 ± 0.0054	(6.5 ± 0.5) × 10^{-25}
3	6177.729 ± 0.004	8.46 ± 0.30	0.0173 ± 0.0042	(4.5 ± 0.5) × 10^{-25}
4	6184.385 ± 0.009	7.92 ± 0.90	0.0178 ± 0.0054	(4.0 ± 0.5) × 10^{-25}
5	6183.009 ± 0.010	7.28 ± 0.83	0.0234 ± 0.0058	(4.5 ± 0.5) × 10^{-25}

absorption features unexplained by solar absorption features (with typical depth below 2% of the continuum and 3σ errorbars of 0.2%) appear to be explained by this synthetic spectrum for an upper atmosphere of Titan with the Dobrijevic et al. (2016) predicted C_3 standard abundance as the observations appear to be entirely explained by the backscattered solar spectrum (blue) at this scale. This allows to rule out at 3σ the existence of C_3 at the abundance of 5.6 × 10^{13} cm^{-2} predicted by the Dobrijevic et al. (2016) photochemical model.

Similar comparison plots between observational, solar and synthetic spectra of Titan were obtained with lower column densities of C_3 abundance in Titan's upper atmosphere, within the range of values predicted by the aforementioned photochemical model (Dobrijevic et al., 2016). Now, we sweep over lower C_3 column density values (between 0 and 2.0×10^{13} cm^{-2}, spaced by intervals of 4.0×10^{12} cm^{-2}) as shown in Fig. 7, with the $N(C_3)$ = 0 cm^{-2} synthetic spectrum corresponding to the aforementioned C_3 OFF, normalised solar spectrum. There appears to be a match between non-solar features in the observational spectrum and the C_3 absorption features of the synthetic spectrum. These modelled C_3 absorption features appear to match at least three weak absorption features at the VLT-UVES spectrum that are not solely explained by solar absorption lines (marked by three red ovals). These absorption features are statistically significant since they differ from the solar spectrum by more than their 3σ errorbars.

Following the example of Dias et al. (2022) detection of chemical species through chemical retrieval of planetary atmospheres, Table 4 lists the wavelength centres of the three absorption features which do not appear to be explained by solar absorption features, comparing their positions to the expected centre of C_3 absorption lines – as

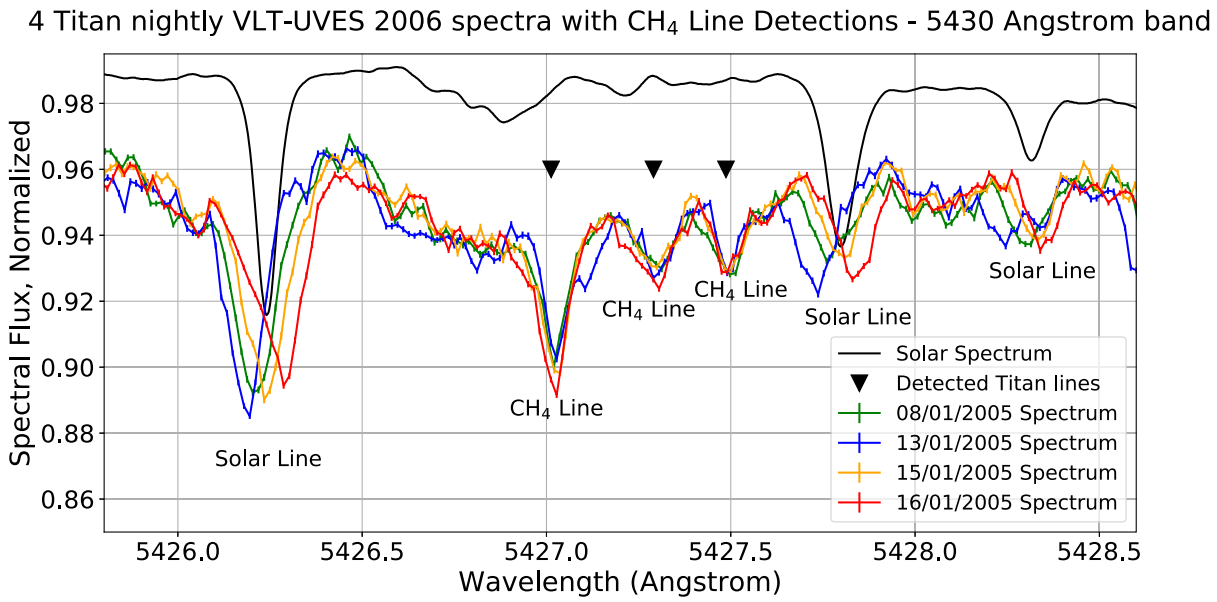

Fig. 4. Line detection with the Doppler Method for Spectral line identification at a section of the weaker 5430 Å CH_4 band, with identification of detected Titan absorption lines with black triangles. In this spectral section we showcase the detection of three non-solar features (most likely Titan CH_4 absorption features) next to three solar lines of similar depth in accordance with the solar spectrum (in black), which, unlike Titan rest frame absorption features, are Doppler shifted due to the relative motion of the Sun and Titan in different observation nights. Errorbars of 3σ are shown, with typical width of 0.2% of the continuum.

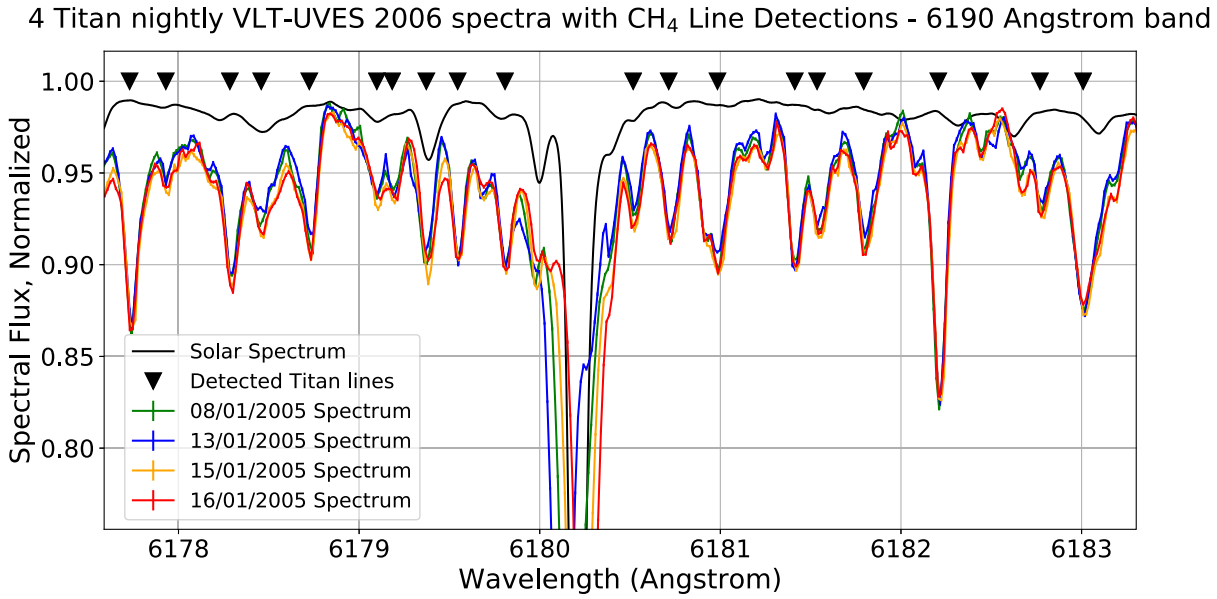

Fig. 5. Line detection with the Doppler Method for Spectral line identification at a section of the 6190 Å CH_4 band. From different nightly spectra with distinct Titan-Sun radial velocities, Solar lines (at 6180.2 Å or at 6183.5 Å) appear shifted in distinct nights of observation, while lines originating from absorption by Titan's atmosphere (uncorrelated to the solar spectrum) do not appear shifted, allowing their detection through our method (marked with black triangles). Errorbars of 3σ are shown, with typical width of 0.2% of the continuum.

Table 4
Non-solar absorption features observed in VLT-UVES blue arm 2018 spectrum of Titan at the spectral range of interest to search for absorption lines part of C_3 4051 Å band (left column) - and possible correspondence to known lines of the $\tilde{A}^1\Pi_u$ - $\tilde{X}^1\Sigma_g^+$ 000–000 absorption band of C_3, from Schmidt *et al* (2014) (Schmidt et al., 2014), including the intrinsic line strengths of the expected C_3 absorption lines that match the position of the three non-solar spectral features.

VLT-UVES line centre (Å)	C_3 line (Schmidt et al., 2014)	C_3 line centre (Å) (Schmidt et al., 2014)	Line strength, S_{ij}, (cm/molec)
Line 1: 4050.18 ± 0.02	R(12)	4050.191 ± 0.010	1.32×10^{-21}
Line 2: 4050.87 ± 0.02	R(4)	4050.857 ± 0.010	1.03×10^{-21}
Line 3: 4051.58 ± 0.02	Q(6)	4051.578 ± 0.010	2.42×10^{-21}

listed in Schmidt et al. (2014) – whose wavelength positions these observed absorption features fall within the wavelength bin uncertainty of 0.02 Å.

All 3 detected non-solar features at the C_3 band region of Titan's spectrum match the position of a Schmidt et al. (2014) C_3 absorption line within their wavelength bin uncertainty (0.02 Å). Titan's

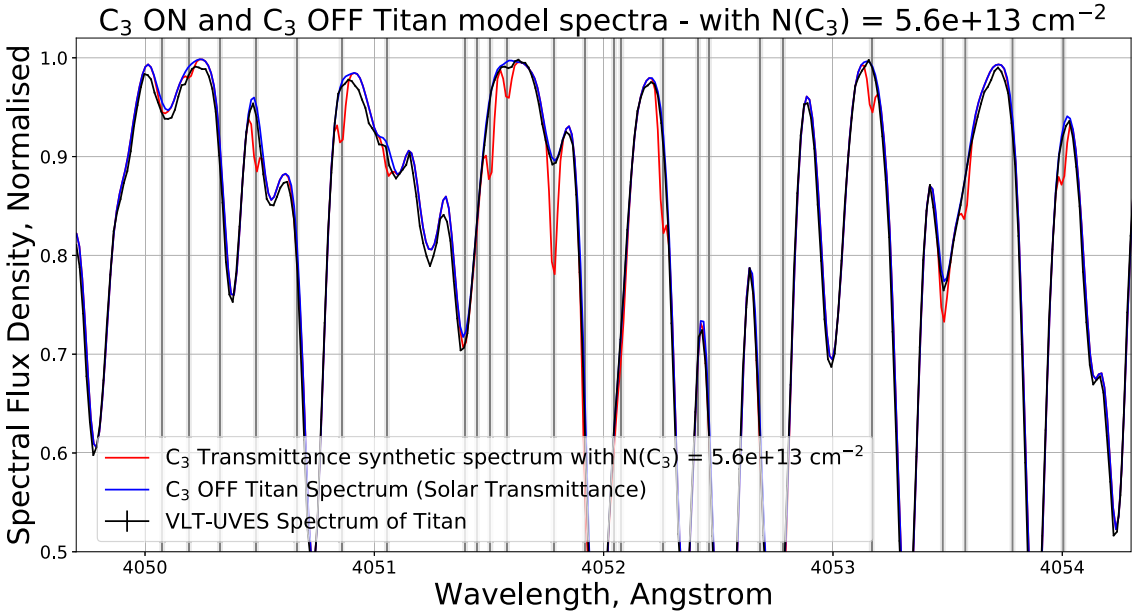

Fig. 6. Normalised Spectrum of Titan (black) compared with a synthetic normalised spectrum of Titan with a C_3 column density of 5.6×10^{13} cm^{-2} (red) and a normalised solar spectrum (blue) as a proxy for a synthetic spectrum of Titan without C_3 absorption features. Vertical grey lines correspond to C_3 line centres and respective uncertainty identified in Schmidt et al. (2014). No observed spectral features appear to match C_3 absorption lines for the standard abundance of this gas predicted by the Dobrijevic et al. (2017) photochemical model (Dobrijevic et al., 2016).

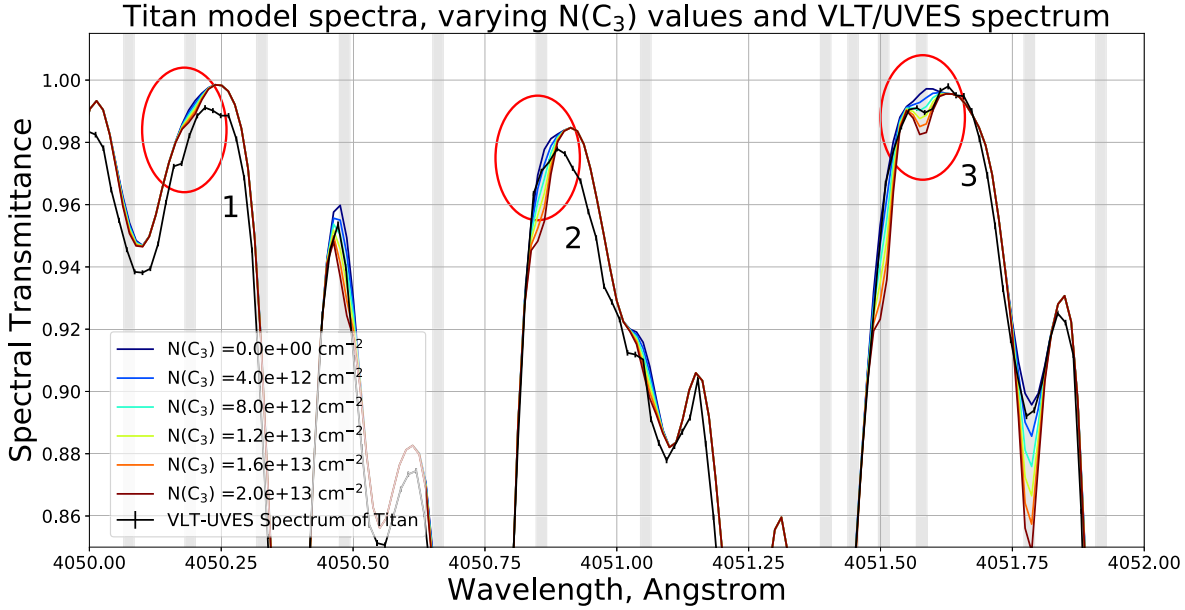

Fig. 7. Normalised Spectrum of Titan (black) compared with synthetic normalised spectra of Titan for several C_3 column densities, N(C_3), sweeping from 0 to $2,0 \times 10^{13}$ cm^{-2}, with steps of $4,0 \times 10^{12}$ cm^{-2}. Vertical grey lines correspond to C_3 line centres and respective uncertainty identified in Schmidt et al. (2014). Red ellipses evidence three possible detections of absorption lines in Titan spectrum that are not explained by backscattered of solar radiation alone — but instead match the expected wavelengths of C_3 absorption lines. Errorbars of 3σ are shown in observational data, with typical width of 0.2% of the continuum.

backscattered spectral features 1 and 3 also appear to match the shape the modelled C_3 lines corresponding to transitions R(12) and Q(6), respectively, of C_3 4051 Å band — whereas spectral feature 2 correlates solely in position with line C_3 band R(4) transition, although its shape differs from the modelled C_3 spectral feature.

At the same time, since all other synthetic C_3 spectral lines fall within deep solar absorption lines, they do not showcase other easily identifiable spectral features of C_3 on the rest of its 4051 Å absorption band — see Figure S2 on Supplementary Information, equivalent to the comparison of VLT-UVES spectrum with the solar and synthetic Titan spectrum with a column density of 1.0×10^{13} cm^{-2} of Fig. 7 but covering the rest of the C_3 4051 Å absorption band, in the wavelength range of 4052 Å to 4055 Å. Examples of such features, which do not appear to be solely explained by the solar spectrum, but that also happen to coincide with deep solar lines are found at (4051,78 ± 0,02) Å, (4053,14 ± 0,02) Å and (4053,68 ± 0,02) Å. It is interesting that 2 of these features also coincide in wavelength to 2 other known C_3 absorption lines: Q(10) at (4051.782 ± 0.010) Å and P(10) at (4053.169 ± 0.010) Å. However, given their coincidence with deep solar lines (deeper than 10% of the continuum), few more considerations can be retrieved from these features as their shape is highly affected by the deep solar lines. Hence, our analysis is more conservative, focusing on the sturdier detection of

the 3 spectral features that match areas free of deep solar lines, all of which coincide in wavelength with known C_3 absorption lines.

The comparison of VLT/UVES Titan spectral features depth with the distinct spectra of varying C_3 column density also allows to provide an estimate of the tentatively detected C_3 disk-integrated average column abundance. The most evident non-solar feature (3, coinciding with C_3 Q(6) line) appears to be better fit in depth by the $N(C_3) = 8,0 \times 10^{12}$ cm^{-2} synthetic spectrum, whereas spectral feature 1 appears to require a larger C_3 abundance (of at least $N(C_3) = 1,6 \times 10^{13}$ cm^{-2}) for the synthetic spectrum to replicate the shape of the observed spectral feature. Furthermore, for spectral feature 2, the synthetic spectrum with $N(C_3) = 4,0 \times 10^{12}$ cm^{-2} appears to better fit the data. Taking into account these results, we estimate a tentative detection of C_3 at a column density of $N(C_3) = (1,0 \pm 0,6) \times 10^{13}$ cm^{-2}.

6. Discussion and conclusions

6.1. High resolution visible CH_4 line identification on Titan's atmosphere

Motivated by the current lack of linelists for visible methane absorption bands below 7460 Å (Hargreaves et al., 2020; Giver, 1978), we have developed a new method to take advantage of the Doppler shift affecting solar lines on four different nightly observations of Titan, and detect previously unknown non-solar absorption lines on spectral regions covered by CH_4 visible bands, amid deeper, backscattered solar lines. This new method shares similarities with the Doppler Tomography technique, used to detect known spectral absorption lines originated in exoplanet atmospheres undergoing sinusoidal Doppler shifts over the course of the exoplanet's orbit (Snellen et al., 2010; Watson et al., 2019). Our method, nonetheless, differs from the Doppler tomography method by aiming to detect previously unknown absorption lines of a chemical species at a planetary atmosphere by distinguishing them from bacskcattered solar absorption features. Hence, unlike the Doppler tomography method, our method is agnostic regarding the wavelengths of the spectral features to be detected, and by being applied to solar system atmospheres, allows the line-by-line characterisation of weak absorption bands inaccessible to laboratory studies (Bourdon et al., 2009). Furthermore, previous works have also measured Doppler shifts on solar absorption lines backscattered from planetary atmospheres through the Doppler velocimetry technique, (Machado et al., 2014; Goncalves et al., 2020), with the goal of retrieving maps of zonal and meridional winds at distinct atmospheric layers — again, a distinct technique for a distinct goal.

Using threshold criteria for detection (maximum line position shift of 25 mÅ between all four observation nights, as well as minimum line depth of 2% of the spectral continuum) a total of 97 non-solar lines were detected at the 5250 Å- 6186 Å spectral range, all of them within the expected spectral sections corresponding to CH_4 visible absorption bands. The vast majority of these detected spectral lines is concentrated at wavelengths above 6100 Å, precisely at the location of the deeper CH_4 visible absorption band Giver (1978). Assessing how detected line depth is distributed as a function of wavelength at the vicinity of this 6190 Å band, we obtain the plot in Fig. 8.

Here we observe that deeper lines progressively cluster closer to the CH_4 band 6190 Å centre, while lines below the 2% relative depth threshold appear more dispersed in wavelength. This may indicate that due to their reduced contrast with respect to the continuum, the line detection algorithm may create spurious line detections — some of which will fit the 1st criteria of proximity in position across nightly spectra. Hence the decision of including a minimum line depth threshold of 2% (5 times the typical line depth measurement uncertainty at 3σ) for line detection, a conservative limit ensuring that detected lines are indeed visually discernible from the solar spectrum.

It is important to generalise the line detection criteria (used in the application of this method to VLT/UVES data) to allow a distinction between planetary and solar absorption lines with other instruments and observational settings. Regarding maximum line separation (here set at 25 mÅ), future applications of this method should select this value based on the minimum Doppler shift between distinct nightly spectra. This Doppler shift should, nonetheless, be greater than the size of the detector's wavelength bin. As for the minimum line depth threshold for line detection (here set at a depth of 2% of the continuum), it should be of at least equal to the value of typical uncertainty of line depth estimation. Finally, regarding the 3rd criterion of distance from a solar line in order to its line strength estimation to be valid: we suggest a minimum distance equal to the detector's spectral resolution (of 60 mÅ in this case) to avoid the contamination of detected planetary line's depth estimations by solar absorption lines.

A literature survey was conducted with the goal of identifying other molecular absorbers on Titan. For trace molecular species on Titan's atmosphere, species such as C_2H_2, C_2H_4, C_2H_6, C_3H_4, C_3H_6, C_3H_8 and heavier hydrocarbons, no absorption bands of these species are included in the HITRAN (Gordon et al., 2022), EXOMOL (Tennyson et al., 2007) or MPI-Mainz UV/VIS Spectral Atlas databases (Keller-Rudek et al., 2013). The same is true for the most abundant Nitrile species such as HC_3N, CH_3CN and C_2N_2. The sole molecular absorbers in Titan's atmosphere with known absorption lines on visible wavelengths probed in search for CH_4 and C_3 absorption lines are (according to the HITRAN database) HCN, CO_2 and CO.

A HCN molecular band is centred at 5710 Å, with maximum line strength of 10^{-25} cm/molec. This is the same line strength as that of the weakest detected CH_4 lines. However, since HCN column density down to the optical radius of Titan (at 200 km) is of 1.4×10^{17} cm^{-2} (following the Teanby et al. (2006) profile (Teanby et al., 2006)). This is smaller than CH_4 column density down to the same level by a factor of the order of 10^4, and thus we expect possible HCN absorption lines to be at least 10^4 × weaker than those of the weakest detected CH_4 lines. It is therefore unlikely that any HCN absorption lines at this Titan spectrum are misinterpreted as CH_4 absorption lines. The same argument can be conveyed for CO_2 and CO, which are also known to have absorption lines near 6000 Å with line strengths below 10^{-29} cm^2, associated with column densities down to 200 km of 5.6×10^{15} cm^{-2} and 7.5×10^{18} cm^{-2}, respectively.

Hence, due to the lack of other known relevant molecular absorbers of the spectral section observed by Luz et al. (2006) on Titan's atmosphere apart from methane (McKay et al., 2001), and given the lack of correspondence between the detected line absorption lines present in the solar spectrum (Figs. 4 and 5) we conclude that the detected lines are not only non-solar and originated in Titan's atmosphere rest frame, but indeed part of the previously uncharacterised visible absorption bands of $^{12}CH_4$.

This work builds upon previous studies that have aimed to retrieve CH_4 visible bands absorption cross sections – with the goal of further constraining CH_4 visible absorption spectrum as a probe to planetary atmospheres – through laboratory studies (Giver, 1978) and with the comparison with observations of solar system CH_4-bearing atmospheres (Smith et al., 1990; Karkoschka and Tomasko, 2010). Giver (1978) has presented a laboratory measurement and vibrational assignment of high overtone CH_4 bands shortward of 1 μm. Hayden Smith et al. (1990) have presented a detailed analysis of the 6190 Å band shape and dependence with temperature in laboratory, and compared it with the observed spectrum of Uranus (Smith et al., 1990). To this day, detailed high resolution line-by-line lists available at spectroscopic databases like HITRAN (Gordon et al., 2022) or ExoMol (Tennyson et al., 2007) still do not cover this section of CH_4 spectrum. More recent works such as Karkoschka and Tomasko (2010) present a further comparison of HST observations of Jupiter and Huygens observations of Titan's spectrum from 0.4 μm to 5 μm with laboratory data, assessing methane absorption coefficients dependence in temperature and pressure, and assessing the differences between laboratory and planetary spectra of CH_4 - at low spectral resolution. Our results present therefore the first identification of CH_4 spectral features at high spectral

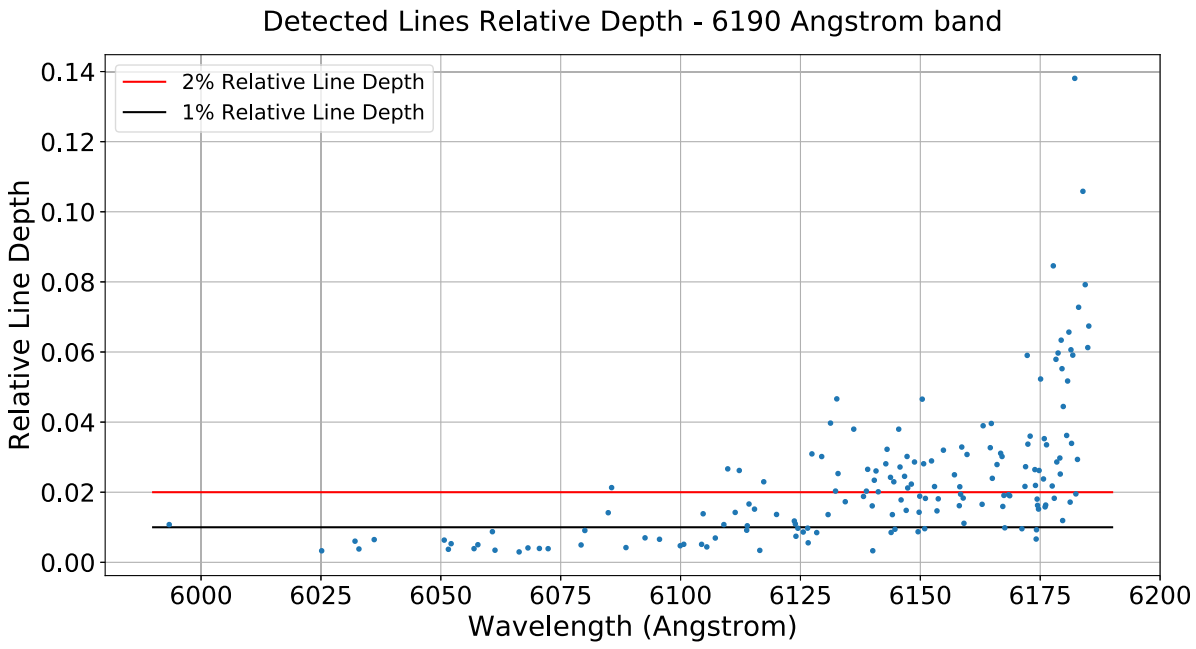

Fig. 8. Detected line depth as a function of wavelength at the region covering the most intense visible CH_4 band (6190 Å band) between 6090 Å and 6186 Å. Deeper detected lines cluster towards the central wavelength of the methane band at 6190 Å (beyond the limits of our spectrum). Weaker lines with depths below 2% of the continuum do not share this clustered nature, suggesting some of them could be spurious line detections. Line detections were therefore considered only for line depths above 2%.

resolution ($R = 100.000$) at 4 methane absorption bands between 5250 Å and 6186 Å from observations of Titan's atmosphere analysed with our new Doppler-based method allowing the distinction between Titan and Solar lines.

This has allowed to associate and explain previously observed at lower resolution ($R = 10,000$ for Giver (1978)) features of the overtone-combination bands $5\nu_1+\nu_3$ (6190 Å), $4\nu_1+2\nu_3$ (5970 Å), $5\nu_1+\nu_3+(\nu_2$ or $\nu_4)$ (5760 Å) and $6\nu_1+\nu_3$ (5430 Å) (Giver, 1978; Smith et al., 1990). One such example is the CH_4 absorption coefficient (κ_{CH_4}) "shoulder" feature at ~ 6175 Å, described in the $5\nu_1+\nu_3$ band by Smith et al. (1990). They observed a steep increase of the absorption coefficient κ_{CH_4} between 6175 Å and 6190 Å by an average of 8×10^{-27} cm^{-2} per Å, following a shallower average increase of κ_{CH_4} between 6125 Å and 6175 Å of 3×10^{-27} cm^{-2} per Å. This tendency is also observed in the line depth distribution plot of Fig. 8, as maximum line depth appears to stagnate between 6125 Å and 6175 Å and increase by a factor of 2 after 6175 Å, where the deeper detected lines seem to cluster, closer to the band centre.

As discussed in Bourdon et al. (2009) and Karkoschka and Tomasko (2010), the use of laboratory studies to probe methane's weak visible absorption lines is challenging given the current difficulty in replicating in laboratory the hundreds of kilometers crossed by light in a planetary atmosphere — that allow visible bands, originated by highly excited CH_4 states, to imprint their absorption on the outgoing planetary spectrum. Empirical work such as this is not able to deliver a complete picture of the complex nature of the visible CH_4 bands through a linelist that can be used for atmospheric modelling in a wide array of planetary atmosphere settings such as the ones provided by HITRAN (Gordon et al., 2022). However, by using high-resolution astrophysical spectroscopy combined to our simple line Doppler characterisation method, we have been able to gather a high-resolution ($R = 100.000$), low Temperature ($T = 150$ K), list of close to 100 CH_4 absorption features between 5250 Å and 6186 Å.

These results provide a helpful base of comparison for future expansions of CH_4 line-lists into shorter wavelengths, such that this first cut at methane parameters in this region may trigger future *ab initio* and laboratory studies aiming at the full determination of the methane spectroscopic parameters in this wavelength range. This characterisation is of particular importance, given the aforementioned geochemical and astrobiological relevance of CH_4 in current and future studies of exoplanet atmospheres, which at extremely high resolutions (reaching $R = 190,000$ as is the case of VLT-ESPRESSO) are still circumscribed to ground-based visible observatories.

6.2. Search for C_3 spectral features on Titan's atmosphere

Following the prolific discovery of new carbon-based species on Titan's atmosphere, and the predictions from new photochemical models (Hérbad et al., 2013; Dobrijevic et al., 2016) we have analysed dedicated VLT-UVES blue arm observations in search for absorption lines of carbon trimer, C_3 4051 Å band on Titan's atmosphere. Comparing the normalised VLT-UVES Titan spectrum with the normalised solar spectrum and first-approximation synthetic C_3 spectrum between 4050 Å and 4055 Å, has provided an upper-limit for C_3 column density on Titan's upper atmosphere below the model-predicted 5.6×10^{13} cm^{-2}.

However, for first-approximation synthetic spectra of Titan sweeping lower C_3 column density values of from 0 to 2.0×10^{13} cm^{-2}, within the model-predicted range of C_3 column densities (Hérbad et al., 2013; Dobrijevic et al., 2016), it was possible to assess the correspondence between three non-solar spectral features on VLT-UVES Titan spectrum and the shape and central wavelengths of three C_3 lines from Schmidt et al. (2014), estimating a C_3 average, disk-integrated column density of $(1.0 \pm 0.6)\times10^{13}$ cm^{-2}.

All three assessed spectral features correspondences occur at the small spectral windows where solar transmittance is flat and close to 1, and therefore relatively free from solar spectral features. This is expected since detection of such weak absorption features (absorbing less than 1% of the incoming flux at the lower limit of C_3 column density) requires the absence of other stronger spectral features, particularly as strong as the solar lines found in this spectral region of interest. It is therefore not surprising that other, possibly stronger, C_3 absorption lines are not found in this spectral range of interest due to the overlap with deeper solar lines — given that these three regions free of solar lines where tentative detections were obtained are among the sole solar line free spectral ranges found in this region of the spectrum, and that match the position of possible C_3 lines.

Apart from solar features, another possible non-C_3 origin for these spectral features could be other molecular absorber in Titan's atmosphere — for instance uncharacterised high energy CH_4 absorption features. The current nonexistence of line-by-line lists for CH_4 at these wavelengths makes it impossible to completely discard CH_4 weak lines as the source of these observed features near 4051 Å. However, it is possible to compare the measured line depths at the 5430 Å CH_4 band with lower resolution (≈ 10 Å) absorption cross-section spectra of methane (for instance, He et al. (2021)) - and infer the maximum expected depth of CH_4 lines near 4051 Å, given methane's absorption measured low-resolution cross-section at this wavelength.

For a low resolution (R = 500) CH_4 absorption coefficient (κ_{CH_4}) of 5×10^{-26} cm/molecule for 5430 Å, and of 2×10^{-27} cm/molecule for 4050 Å, as measured by He et al. (2021) we could expect a maximum line depth of eventual CH_4 lines at the same wavelengths of the C_3 band to be 25 times lower than that of its 5430 Å band. This estimation leads us to expect a maximum line depth of putative CH_4 lines at 4050 Å of 0.15%, which is significantly lower than the 0.5% depths of the non-solar features in Fig. 7. This comparison highlights the importance of the characterisation of CH_4 high resolution visible spectrum when searching for faint visible molecular absorption features of other molecules in Titan's atmosphere.

Although we cannot claim the detection of C_3 in Titan's atmosphere from these observed spectral features, these results are encouraging and compatible with the existence of C_3 in Titan's upper atmosphere with a column density of $(1.0 \pm 0.6) \times 10^{13}$ cm^{-2}. The photochemical model that initiated this search for C_3 in Titan's atmosphere is mainly that of Dobrijevic et al. (2016). In this model, C_3 reaches a fairly high abundance (above ppm levels above altitudes of 600 km) due to its low reactivity. Indeed, C_3 is a quasi-molecule known to have a low reactivity with the abundant molecules present in Titan's atmosphere (N_2, CH_4, C_2H_2, C_2H_4, etc.) (Nelson et al., 1981, 1982). The reactivity of C_3 with radicals assumed to be abundant in Titan's upper atmosphere, such as atomic H and CH_3, is not known but C_3 is assumed not to react quickly with atomic oxygen (Woon et al., 1996), and atomic H and CH_3 are generally much less reactive than atomic O. However, there is considerable uncertainty about the reactivity of C_3 with radicals, and our observational results suggest that this reactivity is in fact much greater than assumed — with a tentatively detected C_3 column density 5 times lower than predicted by Dobrijevic et al. (2016). In this respect, it should be noted that a recent theoretical study on the reaction of C_3 with propargyl C_3H_3 appears to be barrier-free (Mebel et al., 2023), and the authors suggest that C_3 could also react without barrier with CH_3 radical. Clearly, C_3 reactivity with radicals and atoms deserves to be studied in detail.

Further observations are required to advance with a C_3 detection claim. In case this claim is confirmed, it provides a constraint for photochemical products expected to be found on Titan's upper atmosphere above 600 km (as opposed to most sub-mm and infrared spectroscopy detections, which have mostly probed Titan's stratosphere (Lombardo et al., 2019)). Ultra high resolution (R = 190.000) visible observations of Titan, aimed at observing the C_3 absorption band centred at 4051 Å may allow a definitive confirmation of the presence of C_3 absorption features in Titan's spectrum. Taking advantage of our Doppler Line Identification Method presented above in this work, if observed in distinct observation nights, the Doppler shift of solar lines may allow the detection of C_3 in Titan's spectrum if it is enough to shift the solar lines by at least one wavelength bin — compared with fixed possible C_3 lines present in Titan's atmosphere.

Funding

This work was supported by Fundação para a Ciência e Tecnologia (FCT), Portugal through the research grants 2022.09859.BD, and 2021.04584.BD and UIDP/04434/2020 through national funds (PIDDAC). Centro de Química Estrutural acknowledges the financial support of Fundação para a Ciência e Tecnologia (FCT), Portugal through projects UIDB/00100/2020 and UIDP/00100/2020. Institute of Molecular Sciences acknowledges the financial support of Fundação para a Ciência e Tecnologia (FCT), Portugal through project LA/P/005-6/2020.

CRediT authorship contribution statement

Rafael Rianço-Silva: Conceptualization, Data curation, Formal analysis, Investigation, Methodology, Software, Supervision, Validation, Visualization, Writing – original draft, Writing – review & editing. **Pedro Machado:** Conceptualization, Data curation, Formal analysis, Investigation, Methodology, Supervision, Validation, Visualization, Writing – original draft, Writing – review & editing. **Zita Martins:** Conceptualization, Formal analysis, Investigation, Validation, Writing – review & editing. **Emmanuel Lellouch:** Conceptualization, Data curation, Formal analysis, Investigation, Methodology, Validation, Visualization, Writing – review & editing. **Jean-Christophe Loison:** Conceptualization, Data curation, Formal analysis, Investigation, Methodology, Validation, Writing – review & editing. **Michel Dobrijevic:** Conceptualization, Data curation, Formal analysis, Investigation. **João A. Dias:** Data curation, Methodology, Software, Visualization. **José Ribeiro:** Data curation, Methodology, Software, Visualization.

Declaration of competing interest

The authors declare that they have no known competing financial interests or personal relationships that could have appeared to influence the work reported in this paper.

Data availability

Data will be made available on request.

Acknowledgements

This study was based on observations collected at the European Organisation for Astronomical Research in the Southern Hemisphere under ESO programme 074.C-0569 (A) and 0101.C-0573(A).

Appendix A. Supplementary data

Supplementary material related to this article can be found online at https://doi.org/10.1016/j.pss.2023.105836.

References

Aboudarham, J., Renié, C., 2020. BASS2000, database of solar ground-based observations. BASS2000. http://dx.doi.org/10.25935/9TXJ-F095.

Bourdon, V., et al., 2009. Methane in Titan's atmosphere: From fundamental spectroscopy to planetology. Europhys. News 40, 4. http://dx.doi.org/10.1051/epn/2009601.

Cordiner, M., et al., 2015. Ethyl cyanide on Titan: Spectroscopic detection and mapping using ALMA. Astrophys. J. Lett. 800, L14. http://dx.doi.org/10.1088/2041-8205/800/1/L14.

Coustenis, A., et al., 2007. The composition of Titan's stratosphere from Cassini/CIRS mid-infrared spectra. Icarus 189, 35–62, http://dx.doi.org/10.1016/j.icarus.2006.12.022.

D'Aversa, E., et al., 2017. A visible solar occultation of Titan's atmosphere from Cassini-VIMS. In: 19th EGU General Assembly, EGU2017. https://meetingorganizer.copernicus.org/EGU2017/EGU2017-5167.pdf.

Dekker, H., et al., 2000. Design, construction and performance of UVES, the echelle spectrograph for the UT2 Kueyen telescope at the ESO paranal. In: Proc. SPIE 4008, Optical and IR Telescope Instrumentation and Detectors. http://dx.doi.org/10.1117/12.395512.

Dias, J., et al., 2022. From atmospheric evolution to the search of species of astrobiological interest in the solar system—Case studies using the planetary spectrum generator. Atmosphere 13, http://dx.doi.org/10.3390/atmos13030461.

Dobrijevic, M., et al., 2016. 1-d coupled photochemical model of neutrals, cations and anions in the atmosphere of titan. Icarus 268, 313–339. http://dx.doi.org/10.1016/j.icarus.2015.12.045.

Encrenaz, T., et al., 2010. The Solar System. Springer-Verlag Berlin Heidelberg, New York.
Formisano, V., et al., 2004. Detection of methane in the atmosphere of Mars. Science 306, http://dx.doi.org/10.1126/science.1101732.
Gausset, L., et al., 1965. Analysis of the 4050-Å group of the C_3 molecule. Agron. J. 142:45.
Gialluca, M., et al., 2021. Characterizing atmospheres of transiting Earth-like exoplanets orbiting M Dwarfs with James Webb space telescope. Publ. Astron. Soc. Pac. 133, http://dx.doi.org/10.1088/1538-3873/abf367.
Giver, L., 1978. Intensity measurements of the CH4 bands in the region 4350Å to 10600Å. J. Quant. Spectrosc. Radiat. Transfer 19, http://dx.doi.org/10.1016/00224073(78)90064-X.
Goncalves, R., et al., 2020. Venus' cloud top wind study: Coordinated Akatsuki/UVI with cloud tracking and TNG/HARPS-N with Doppler velocimetry observations. Icarus 335, http://dx.doi.org/10.1016/j.icarus.2019.113418.
Gordon, I., et al., 2022. The HITRAN2020 molecular spectroscopic database. J. Quant. Spectrosc. Radiat. Transfer 277, http://dx.doi.org/10.1016/j.jqsrt.2021.107949.
Hanel, R., et al., 2003. Exploration of the Solar System By Infrared Remote Sensing, second ed. Cambridge University Press.
Hargreaves, R., et al., 2020. An accurate, extensive, and practical line list of methane for the HITEMP database. Astrophys. J. Suppl. Ser. 247:55, http://dx.doi.org/10.3847/1538-4365/ab7a1a.
He, Q., et al., 2021. Scattering and absorption cross sections of atmospheric gases in the ultraviolet–visible wavelength range (307–725nm). Atmos. Chem. Phys. 21, http://dx.doi.org/10.5194/acp-21-14927-2021.
Hérbad, E., et al., 2013. Photochemistry of C_3Hp hydrocarbons in Titan's stratosphere revisited. Astron. Astrophys. 552, A132.
Hinkle, K., et al., 1988. Detection of C_3 in the circumstellar shell of IRC+10216. Science 241, http://dx.doi.org/10.1126/science.241.4871.1319.
Hörst, S.M., 2017. Titan's atmosphere and climate. J. Geophys. Res.: Planets 122, http://dx.doi.org/10.1002/2016JE005240.
Hörst, S.M., et al., 2012. Formation of amino acids and nucleotide bases in a Titan atmosphere simulation experiment. Astrobiology 12, http://dx.doi.org/10.1089/ast.2011.0623.
Irwin, P., et al., 2008. The NEMESIS planetary atmosphere radiative transfer and retrieval tool. J. Quant. Spectrosc. Radiat. Transfer 109, http://dx.doi.org/10.1016/j.jqsrt.2007.11.006.
Karkoschka, E., 1994. Spectrophotometry of the Jovian planets and Titan at 300- to 1000-nm wavelength: The methane spectrum. Icarus 111:1, http://dx.doi.org/10.1006/icar.1994.1139.
Karkoschka, E., Tomasko, M., 2010. Methane absorption coefficients for the Jovian planets from laboratory, Huygens, and HST data. Icarus 205, http://dx.doi.org/10.1016/j.icarus.2009.07.044.
Keller-Rudek, H., et al., 2013. The MPI-Mainz UV/VIS spectral atlas of gaseous molecules of atmospheric interest. Earth Syst. Sci. Data 5, http://dx.doi.org/10.5194/essd-5-365-2013.
Krasnopolsky, V., et al., 2004. Detection of methane in the martian atmosphere: Evidence for life? Icarus 172:2, http://dx.doi.org/10.1016/j.icarus.2004.07.004.
Krissansen-Totton, J., et al., 2018. Disequilibrium biosignatures over earth history and implications for detecting exoplanet life. Sci. Adv. 4, http://dx.doi.org/10.1126/sciadv.aao5747.
Lellouch, E., et al., 2022. Pluto's atmosphere observations with ALMA: Spatially-resolved maps of CO and HCN emission and first detection of HNC. Icarus 372, http://dx.doi.org/10.1016/j.icarus.2021.114722.
Lombardo, N., et al., 2019. Detection of propadiene on Titan. Astrophys. J. Lett. 881:L33, http://dx.doi.org/10.3847/20418213/ab3860.
Lorenz, R., et al., 1999. Seasonal change on Titan observed with the hubble space telescope WFPC-2. Icarus 142, http://dx.doi.org/10.1006/icar.1999.6225.
Luz, D., et al., 2006. Characterization of zonal winds in the stratosphere of Titan with UVES: 2. Observations coordinated with the Huygens probe entry. J. Geophys. Res. 111, http://dx.doi.org/10.1029/2005JE002617.
Machado, P., et al., 2014. Wind circulation regimes at Venus' cloud tops: Ground-based Doppler velocimetry using CFHT/ESPaDOnS and comparison with simultaneous cloud tracking measurements using VEx/VIRTIS in February 2011. Icarus 243, http://dx.doi.org/10.1016/j.icarus.2014.08.030.
McKay, C., et al., 2001. Physical properties of the organic aerosols and clouds on Titan. Planet. Space Sci. 49, http://dx.doi.org/10.1016/S0032-0633(00)00051-9.
Mebel, A., et al., 2023. Elucidating the formation of ethynylbutatrienylidene (HCC-CHCCC; X^1A') in the Taurus molecular cloud (TMC-1) via the gas-phase reaction of tricarbon (C3) with the propargyl radical (C3H3). Astrophys. J. Lett. 945, L40. http://dx.doi.org/10.3847/2041-8213/acbf41.
Nelson, H., et al., 1981. Reactions of C3 with alkenes, alkynes and allenes. Chem. Phys. 60, http://dx.doi.org/10.1016/0301-0104(81)80120-6.
Nelson, H., et al., 1982. Temperature dependence of C3($X^1\Sigma_g^+$) reactions with alkenes and alkynes, 295-610 K. Chem. Phys. 73, 3. http://dx.doi.org/10.1016/0301-0104(82)85182-3.
Nixon, C., et al., 2013. Detection of propene in Titan's stratosphere. Astrophys. J. Lett. 776:L14, 6pp. http://dx.doi.org/10.1088/2041-8205/776/1/L14.
Nixon, C., et al., 2020. Detection of cyclopropenylidene on Titan with ALMA. Astron. J. 160, http://dx.doi.org/10.3847/15383881/abb679.
Palmer, M., et al., 2017. ALMA detection and astrobiological potential of vinyl cyanide on Titan. Sci. Adv. 3, http://dx.doi.org/10.1126/sciadv.1700022.
Roueff, E., et al., 2002. Interstellar C_3 towards HD 210121. Astron. Astrophys. 384, http://dx.doi.org/10.1051/0004-6361:20020067.
Sánchez-Lavega, A., 2011. An Introduction to Planetary atmospheres. Taylor & Francis.
Schmidt, M., et al., 2014. Detection of vibronic band of C_3 in a translucent cloud towards HD 169454. Mon. Not. R. Astron. Soc. 441, http://dx.doi.org/10.1093/mnras/stu641.
Smith, W.H., et al., 1990. Absorption coefficients for the 6190-Å CH4 band between 290 and 100K with application to Uranus' atmosphere. Icarus 85, http://dx.doi.org/10.1016/0019-1035(90)90103-G.
Snellen, I., et al., 2010. The orbital motion, absolute mass and high-altitude winds of exoplanet HD 209458b. Nature 465, 1049–1051. http://dx.doi.org/10.1038/nature09111.
Tanabashi, A., et al., 2005. Fourrier transform emission of the (000)-(000) band of the λ4051.6 band of C_3. Astrophys. J. 624:2, http://dx.doi.org/10.1086/429316.
Teanby, N., et al., 2006. Latitudinal variations of HCN, HC_3N, and C_2N_2 in Titan's stratosphere derived from Cassini CIRS data. Icarus 181, http://dx.doi.org/10.1016/j.icarus.2005.11.008.
Tennyson, J., et al., 2007. The ExoMol project: Software for computing large molecular line lists. Int. J. Quantum Chem. 117, 92–103. http://dx.doi.org/10.1002/qua.25190.
Thompson, M., et al., 2022. The case and context for atmospheric methane as an exoplanet biosignature. Proc. Natl. Acad. Sci. USA 119:14, http://dx.doi.org/10.1073/pnas.2117933119.
Tinetti, G., et al., 2018. A chemical survey of exoplanets with ARIEL, in experimental. Exp. Astron. 46, http://dx.doi.org/10.1007/s10686-018-9598-x.
Tobie, G., et al., 2009. Evolution of Titan and implications for its hydrocarbon cycle. Philos. R. Soc. 367, http://dx.doi.org/10.1098/rsta.2008.0246.
Villanueva, G., et al., 2018. Planetary spectrum generator:An accurate online radiative transfer suite for atmospheres, comets, small bodies and exoplanets. J. Quant. Spectrosc. Radiat. Transfer 217, http://dx.doi.org/10.1016/j.jqsrt.2018.05.023.
Vuitton, V., et al., 2019. Simulating the density of organic species in the atmosphere of Titan with a coupled ion-neutral photochemical model. Icarus 324, 120–197. http://dx.doi.org/10.1016/j.icarus.2018.06.013.
Watson, C., et al., 2019. Doppler tomography as a tool for detecting exoplanet atmospheres. Mon. Not. R. Astron. Soc. 490, 2. http://dx.doi.org/10.1093/mnras/stz2679.
Woon, D., et al., 1996. On the stability of interstellar carbon clusters: The rate of the reaction between C3 and O. Chem. Phys. 465, http://dx.doi.org/10.1086/177463.